Editors' Suggestion | Featured in Physics

Balancing Information and Dissipation with Partially Observed Fluctuating Signals

Giorgio Nicoletti,[1,*] Ivan Di Terlizzi,[2,3,†] and Daniel Maria Busiello[2,4,‡]

[1]Quantitative Life Sciences section, The Abdus Salam International Center for Theoretical Physics (ICTP), Trieste, Italy
[2]Max Planck Institute for the Physics of Complex Systems, Dresden, Germany
[3]Ludwig-Maximilians-Universität München, Arnold-Sommerfeld-Center for Theoretical Physics, München, Germany
[4]Department of Physics and Astronomy "Galileo Galilei," University of Padova, Padova, Italy

(Received 13 January 2026; accepted 13 July 2026; published 14 September 2026)

Biological systems sense and extract information from fluctuating signals while operating under energetic constraints and limited resolution. We introduce a general chemical model in which a signaling pathway is activated by hidden signals and produces a readout molecule. A sensor, here modeled as an abstract optimization agent, is coupled to the signaling process and can tune the readout production. We propose viable strategies for the sensor to estimate, and eventually balance, information gathering on the hidden process and the associated dissipative cost relying solely on counting statistics of observed trajectories. We show that these strategies can be successfully implemented to adapt the readout production even with finite-time measurements and limited dynamic resolution, and remain effective in the presence of inhibitory regulatory mechanisms. Our Letter provides a plausible mechanism to actively balance information and dissipation, paving the way for an implementable design principle underpinning biological and biochemical adaptation.

DOI: 10.1103/8gx2-rbns

Biological and synthetic systems often rely on noisy fluctuating signals to guide their behavior [1–5]. Cells, for instance, infer environmental conditions and act accordingly by monitoring the stochastic activity of molecular receptors, whose responses are inherently limited by finite dynamic range [6,7], biochemical noise [8–10], and energetic constraints [11–15]. Similar challenges arise in metabolic pathways modulating their propensity to varying nutrient concentrations [16,17], and adaptive materials in which only a distorted trace of the underlying nonequilibrium dynamics is accessible to engineered sensors [18,19]. In all such cases, the system has to tune the strength of its coupling to the signal, whether it is implemented via chemical or mechanical interactions, balancing the information it can extract with the energetic cost of probing [20–25]. A crucial feature to establish robust functioning is that these operations have to be performed in real time, based solely on data that can be directly observed.

Quantifying this balance from stochastic trajectories proves particularly difficult in realistic scenarios, i.e., when the relevant degrees of freedom (d.o.f.) are only partially observable, and the sensing channel has limited resolution. In cellular signaling, for example, the presence of multiple intermediate processing stages hinders direct observations of receptor binding activity [26–28], while saturation effects in enzymatic dynamics and chemical noise can alter the sensitivity to ligand concentration [29,30]. Recent work [21] has shown that approximate estimates of energy consumption during probing can lead to counterintuitive sensing regimes, including cases where an imperfect observer harvests more information than an ideal one, or fails to harvest any information at all. These results underscore the central role of energetics in shaping sensing strategies. Despite providing an interesting proof of concept, the approach presented in [21] remains theoretical, as it relies on force estimation, an inherently challenging task. However, leveraging a recent method to infer dissipation from accessible trajectories using kinetic quantities [31] would open the way to applying these ideas to real biological and synthetic sensing systems.

In this Letter, we consider a hidden chemical process that stimulates the production of a readout molecule via a transduction channel. A sensor, whether chemical or mechanical, can measure the states of both the readout and the transduction signal, e.g., a receptor binding dynamics or a signaling molecule. Rather than specifying a chemical motif for the sensor, we model it as an abstract agent whose objective is to infer, and eventually maximize,

*Contact author: gnicolet@ictp.it
†Contact author: ivandt@pks.mpg.de
‡Contact author: danielmaria.busiello@unipd.it

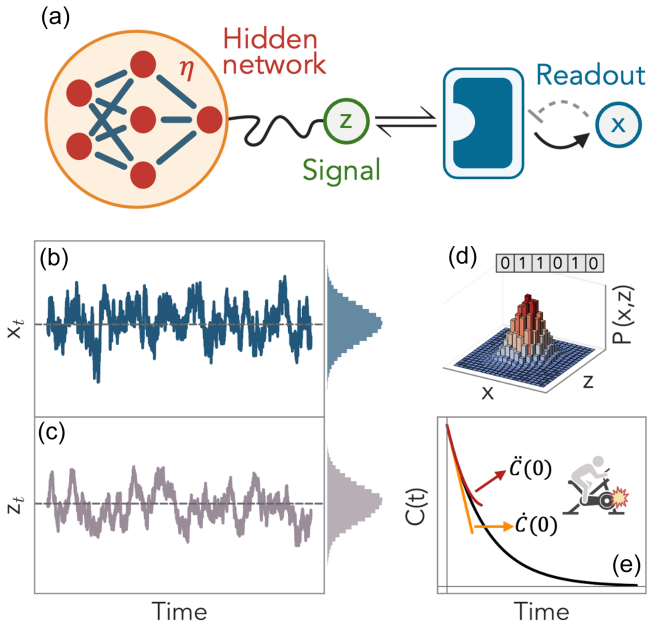

FIG. 1. (a) Schematic of the sensing architecture. A sensor attempts to gather information about the fluctuations $\boldsymbol{\eta}(t)$ of a hidden network, through a readout molecule X coupled to an intermediate signaling molecule Z through receptor binding dynamics. (b),(c) Example trajectories of the fluctuations of the intermediate signal $z(t)$ and the corresponding readout $x(t)$. (d) Empirical joint distribution p_{xz}^{emp} constructed from the observed trajectories to estimate information [Eq. (4)]. (e) Estimation of the traffic $\mathcal{T}_x$ from the short-time curvature of the autocorrelation function, providing an operational measure of the energetic cost of sensing [Eqs. (6) and (7)].

the information between the readout and the hidden chemical population, while controlling the overall energetic cost. Crucially, it must do so directly from the trajectories of the d.o.f. it interacts with, relying solely on counting statistics encoded through empirical distributions and finite differences. This framework allows us to characterize how partial observability shapes the optimal balance between information acquisition and dissipation under realistic, real-time physical constraints.

We focus on a chemical signaling process, which we sketch in Fig. 1(a). A hidden chemical network stimulates the production of a signaling molecule Z, which in turn binds to a membrane receptor to produce an internal readout X. This model can be described by the following set of Langevin equations for concentrations [32]:

$$\begin{aligned}\dot{H}_i &= A_i^{(H)}(\boldsymbol{H}) + \boldsymbol{b}_i^{(H)}(\boldsymbol{H})\cdot\boldsymbol{\xi}_H,\\ \dot{Z} &= A^{(Z)}(\boldsymbol{H},Z,X) + b^{(Z)}(\boldsymbol{H},Z,X)\xi_Z,\\ \dot{X} &= A^{(X)}(Z,X) + b^{(X)}(Z,X)\xi_X,\end{aligned} \tag{1}$$

where H_i are the concentrations of the hidden molecules. They interact both deterministically via a nonlinear force field with components $A_i^{(H)}$ and through their fluctuations, as $\boldsymbol{b}_i^{(H)}$ is a concentration-dependent vector mixing uncorrelated white noises $\boldsymbol{\xi}_H$ coming from different hidden reactions. Conversely, Z and X represent the species accessible to the sensor. These d.o.f. only feature one noise source each (ξ_Z and ξ_X with amplitudes $b^{(Z)}$ and $b^{(X)}$) and nonreciprocal deterministic interactions ($A^{(Z)}$ and $A^{(X)}$). In the End Matter, we show how Eq. (1) can be derived from the exemplary chemical model described above by integrating out the (fast) dynamics of intermediate complexes.

We are interested in how the sensor reads and processes the fluctuations of concentrations (lowercase letters, η_i, z, and x) around the stationary state. Therefore, we employ a linear noise approximation [33,34], ending up with

$$\begin{aligned}\dot{\boldsymbol{\eta}} &= \tau_\eta^{-1}\boldsymbol{W}_\eta\boldsymbol{\eta} + \sqrt{2\boldsymbol{D}_\eta}\boldsymbol{\xi}_\eta,\\ \dot{z} &= -\tau_z^{-1}z + \boldsymbol{\sigma}\cdot\boldsymbol{\eta} + \alpha a x + \sqrt{2D_z}\xi_z,\\ \dot{x} &= -\tau_x^{-1}x + a g(z) + \sqrt{2D_x}\xi_x,\end{aligned} \tag{2}$$

where $\boldsymbol{\xi}_\eta$, ξ_z, and ξ_x are uncorrelated white noises, and τ_η, τ_z, and τ_x characteristic timescales. D_z and D_x are diffusion coefficients that depend in principle on the deterministic fixed points of Eq. (1), and $\boldsymbol{D}_\eta$ and $\tau_\eta^{-1}\boldsymbol{W}_\eta$ are the diffusion and the interaction matrices governing the fluctuations of the hidden d.o.f. The vector $\boldsymbol{\sigma}$ captures the rate of production of the signaling molecule Z, which we also call the signaling rate, while a is the rate of production of the readout X, which we refer to below as the readout coupling. Whenever X is produced, it can feed back on the dynamics of Z through the receptor, e.g., implementing regulatory inhibition mechanisms [22,35–40] [see the gray arrow in Fig. 1(a)]. In Eq. (2), this phenomenon is encoded in α, with $\alpha < 0$ indicating inhibition. We start by taking $\alpha = 0$, i.e., the signaling process cannot be influenced by its readout, but we will relax this assumption further on. Moreover, on top of the linear noise approximation dynamics, we introduce a phenomenological coupling between Z and X as

$$g(z) = r\tanh\left(\frac{z}{r}\right), \tag{3}$$

where r represents the resolution with which the readout can resolve the signal. If $r \to \infty$, g becomes a linear function, whereas for small r, X can only detect small fluctuations. This finite resolution, while approximate, may be relevant in more general settings, such as chemical systems with kinetic traps or catalytic couplings, and models of gene activity [41,42].

The sensor has no direct access to the statistics of $\boldsymbol{\eta}$. Rather, at any time t, it can only measure the fluctuations of the readout, $x(t)$, and that of the signal $z(t)$ [Figs. 1(b) and 1(c)]. Despite being abstract, a concrete realization of such a sensor might be an enzyme converting X into a molecule triggering allosteric changes in the membrane receptor.

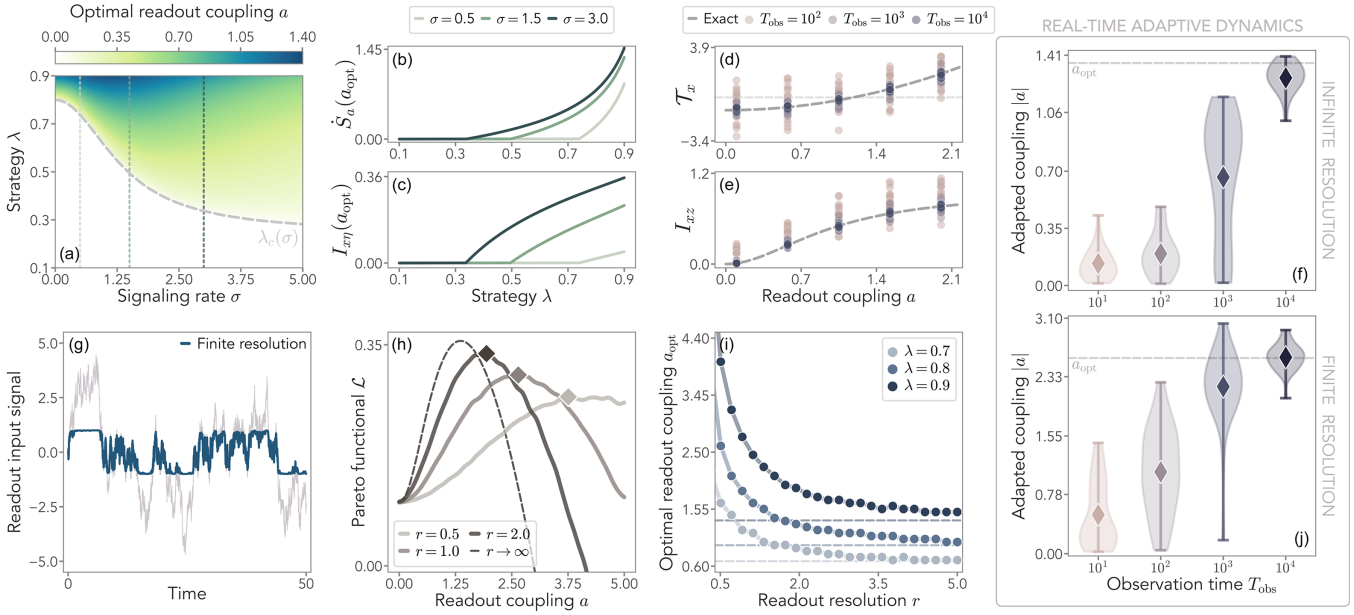

FIG. 2. (a) Optimal readout coupling $a_{\rm opt}$ for infinite resolution as a function of the strategy λ and signaling rate σ. At fixed σ, we find a transition from a regime where $a_{\rm opt}$ vanishes at low λ and increases for $\lambda > \lambda_c$ (gray dashed line). (b),(c) Entropy production, $\dot{S}_a$, and information between x and η, $I_{x\eta}$, as a function of the strategy λ for different values of σ, when $a = a_{\rm opt}$. (d) Estimate of $\mathcal{T}_x$ from trajectories of finite duration $T_{\rm obs}$. As $T_{\rm obs}$ increases, the estimated value approaches the theoretical one (gray dashed line). (e) Same, but for the information between the readout and the signal, I_{xz}. (f) Adapted readout coupling after 10^4 steps of adaptive dynamics, where the sensor attempts to tune a by estimating $\mathcal{T}_x$ and I_{xz} from measurement windows of duration $T_{\rm obs}$. For large enough $T_{\rm obs}$, the readout achieves a near-optimal coupling. Distributions are obtained over 64 repetitions of the adaptive dynamics. (g) Example of the readout input signal, both for infinite resolution (gray trajectory) and for a resolution $r = 1$ (blue trajectory). (h) Comparison of the functional $\mathcal{L}$ at different resolution values. The maximum (triangles) moves at higher values of a as r decreases. (i) Optimal readout coupling as a function of the resolution. As the resolution increases, $a_{\rm opt}$ decreases until it reaches the $r \to \infty$ limit (dashed lines). (j) Same as (f), but for a finite resolution ($r = 1$). In this figure, unless otherwise specified, $D_i = 1/\tau_i$ for $i = \eta, z, x$, $W_\eta = -1$, $\sigma = 1.5$, $\lambda = 0.9$, $\tau_\eta = 3\tau_z$, $\tau_z = \tau_x = 1$.

Such a sensor could indeed record X and Z through direct interaction, and tune the coupling a by accelerating or slowing down the production of X via allosteric mechanisms [43]. Independently of the specific implementation, from these limited observations, the sensor can set a in such a way that it gathers as much information as possible on $\boldsymbol{\eta}$, while at the same time balancing this information gain with the energy it dissipates to achieve it. The sensor can obtain a fluctuating measure of the information between $x(t)$ and $z(t)$ by the pointwise mutual information [14,21],

$$i_{xz}(t) = \log \frac{p_{xz}^{\rm emp}(x(t), z(t))}{p_x^{\rm emp}(x(t)) p_z^{\rm emp}(z(t))}, \tag{4}$$

with $p_{xz}^{\rm emp}$ the joint empirical distribution [Fig. 1(d)], and $p_x^{\rm emp}$ and $p_z^{\rm emp}$ the marginal ones. The mutual information between x and z is the average of Eq. (4) over the observable times, i.e., $I_{xz} = \langle i_{xz} \rangle$. We remark that there is no guarantee *a priori* that increasing I_{xz} will also increase the mutual information between x and $\boldsymbol{\eta}$, $I_{x\boldsymbol{\eta}}$. Nevertheless, as we will see, this is often an effective strategy that allows the sensor to tune the readout production so that it reflects the activity of $\boldsymbol{\eta}$.

Being nonreciprocal, the coupling a leads to unavoidable dissipation [44–50]. A direct evaluation of the associated entropy production $\dot{S}$ is highly challenging, as it would require, in principle, estimating the force field between X and Z from stochastic trajectories [51,52].

To overcome these practical difficulties, we employ a kinetic decomposition of entropy production [31,52,53],

$$\dot{S} = 4\mathcal{T} + \mathcal{G}, \tag{5}$$

which separates dissipation into two contributions accessible from trajectory data. The traffic $\mathcal{T}$ corresponds to the time-symmetric contribution of the path probability relative to a reference drift-free process with the same noise realization [53]. It thus quantifies the excess dynamical fluctuations induced by the forces, while the inflow rate $\mathcal{G}$ [54] captures the local contraction or expansion of probability in phase space due to the drift.

Operationally, $\mathcal{T}$ can be inferred from the short-time curvature of correlation functions, which has been shown

to encode information about dissipation [31,55,56] [see Fig. 1(e)]. For a diagonal diffusion matrix, this yields

$$\mathcal{T} = \sum_i \mathcal{T}_i \qquad 4\mathcal{T}_i = \frac{\ddot{C}_i^{(r)}(t=0)}{\dot{C}_i^{(r)}(t=0)}, \tag{6}$$

with the observed trajectory $\boldsymbol{r}(t) = \{\boldsymbol{\eta}(t), z(t), x(t)\}$ and

$$C_i^{(r)}(t) = \langle r_i(t) r_i(0)\rangle - \langle r_i\rangle^2, \tag{7}$$

the autocorrelations of $\boldsymbol{r}(t)$. In our system (2), the inflow rate is independent of the coupling a (see End Matter), so that variations in dissipation are fully captured by the change in traffic. In particular, the relevant contribution is $\mathcal{T}_x$, which can be extracted directly from the fluctuations of the readout X.

Having measured both information and dissipation from observed fluctuating trajectories, the sensor can implement a strategy λ to balance them. Following previous work [21], we introduce the Pareto functional [57],

$$\mathcal{L}(a,\lambda) = \lambda \langle i_{xz}\rangle(a) - 4(1-\lambda)\mathcal{T}_x(a), \tag{8}$$

where $\lambda \in [0,1]$, and both I_{xz} and $\mathcal{T}_x$ depend on the coupling strength a [see Eq. (3)]. At a given strategy λ, we set the value of a that maximizes information while keeping dissipation as low as possible, i.e., $a_{\mathrm{opt}}(\lambda) = \mathrm{argmax}_a \mathcal{L}(a,\lambda)$. For small λ, the sensor acts to preferentially minimize the estimated dissipation, whereas large λ denotes an information-driven strategy that may incur a higher energetic cost. We stress that the functional in Eq. (8) only contains quantities that are measurable by the sensor.

We first focus on the ideal case of an infinite resolution $r \to \infty$, where the sensor can measure the entire dynamic range of z for an infinite observation window, $T_{\mathrm{obs}} \to \infty$. In this case, Eq. (2) can be solved exactly, so that $\mathcal{L}(a)$ can be obtained analytically. Moreover, for simplicity, we set $\boldsymbol{\eta}$ to be one-dimensional, but the proposed approach can be extended to high-dimensional inaccessible d.o.f. In Fig. 2(a), we show that $a_{\mathrm{opt}}(\lambda)$ displays a sharp transition at $\lambda = \lambda_c(\sigma)$, at all values of σ. Indeed, when the strategy is dissipation-driven (small λ), optimal balance prescribes that no information is harvested, and a_{opt} vanishes. However, as λ increases, the strategy becomes more information-driven, and the optimal coupling eventually becomes nonzero and grows accordingly. Crucially, increasing the strategy λ over a critical value λ_c also corresponds to an increase in the information between the readout $x(t)$ and the underlying hidden process $\eta(t)$, $I_{x\eta}$, while keeping the entropy production induced by the readout coupling, $\dot{S}_a = \dot{S} - \dot{S}|_{a=0}$, as low as possible [see Figs. 2(b) and 2(c)]. This shows that the sensor can construct—and ultimately optimize—efficient representations of information about the inaccessible process and dissipation using only empirical statistics on observed quantities.

When T_{obs} is finite, however, both Eqs. (4) and (7) suffer from sampling errors. Importantly, this closely resembles the common situation of a sensor that must act on the fly. To model this situation, we now consider the case of a sensor that continuously changes a for N adaptation steps of duration T_{obs} each. During the nth step, the sensor sets $a = a_n$ and constructs an estimate of the quantities in Eq. (8) by observing trajectories for the finite time window. Then, the sensor changes the coupling to $\tilde{a}_{n+1} = a_n + \Delta a$, with $\Delta a \sim \mathcal{N}(0,\sigma_a)$ and performs a new trajectory-based estimation of Eqs. (4) and (6). Based on this temporally constrained observation, the new coupling is accepted ($a_{n+1} = \tilde{a}_{n+1}$) if $\mathcal{L}(\tilde{a}_{n+1}) > \mathcal{L}(a_n)$, otherwise the coupling goes back to the previous value ($a_{n+1} = a_n$). This adaptive dynamics proceeds until no new adaptive move is accepted for a sufficiently long stopping time. Notice that we start from a perfectly inhibiting sensor that impedes $x(t)$ from having any information on $\boldsymbol{\eta}(t)$, $a_0 = 0$. First, in Figs. 2(d) and 2(e), we show that, if T_{obs} is particularly small, sampling errors may lead to a large variance in the estimation of both $\mathcal{T}_x$ and I_{xz}, especially at large a. Then, in Fig. 2(f) we plot the distribution of a at convergence of the adaptive dynamics as a function of T_{obs}. Remarkably, as T_{obs} increases, the average of the distribution approaches a_{opt}, allowing the sensor to reach the optimal coupling through purely trajectory-based estimates.

We now move to the case where r is finite, and thus the readout has access to a limited range of values of $z(t)$ [see Fig. 2(g)]. In this case, the phenomenological dynamics is nonlinear and does not admit an exact solution. Nevertheless, in Fig. 2(h) we show that the shape of the Pareto functional remains qualitatively similar to the $r \to \infty$ limit, with the optimal coupling increasing as the resolution decreases. Thus, due to the limited resolution, the readout has to be more strongly coupled to the incoming signal to achieve optimal performance [see Fig. 2(i)]. Crucially, since our trajectory-based approach relies solely on counting statistics, the sensor can still build estimates of the Pareto functional after observing the system for a time T_{obs}, and adapt a accordingly. In Fig. 2(h), we show that the adaptive dynamics allows the sensor to achieve the optimal coupling a_{opt}, as before, for sufficiently long observation times.

An important ingredient in most signaling networks is the presence of regulatory inhibition mechanisms [22,35–39] coupling the readout X with the signaling molecule Z, encoded in the parameter $\alpha < 0$ in Eq. (2). For simplicity, in this scenario, we focus on the infinite resolution limit, $r \to \infty$, as it does not qualitatively change the results. Because of this feedback coupling, the sensor must now estimate dissipation by evaluating the traffic for both the observable d.o.f., $\mathcal{T}_x$ and $\mathcal{T}_z$, defined by their autocorrelation functions [see Eq. (6) and End Matter]. Since the sensor has access to the trajectories of both the

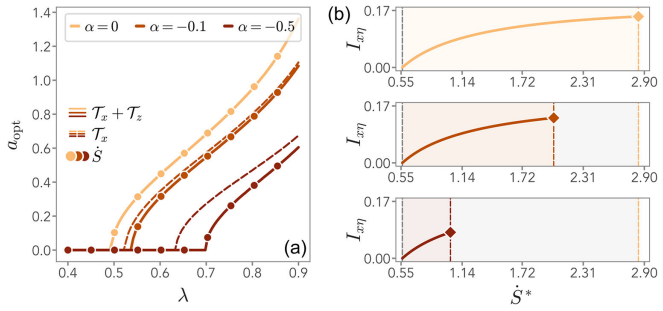

FIG. 3. (a) Optimal readout coupling $a_{\rm opt}$ as a function of the strategy λ. Without an inhibitory feedback coupling ($\alpha = 0$), it is enough to estimate the x component of the traffic $\mathcal{T}_x$, which contains all relevant dependences of $\dot{S}$ on a. When $\alpha < 0$, both $\mathcal{T}_x$ and $\mathcal{T}_z$ are needed, since the functional with the x component alone overestimates $a_{\rm opt}$. As before, there is a critical λ_c below which $a_{\rm opt} = 0$. (b) Information between readout and hidden d.o.f., $I_{x\eta}$, as a function of the energy consumption $\dot{S}^*$ of the system, which is the entropy production at the corresponding optimal coupling $a_{\rm opt}$. Here, $\lambda \in [0.1, 0.9]$. Since $a_{\rm opt}$ decreases with more negative values of α, so does the energy consumption. Thus, the maximum value of $\dot{S}^*$ (squares) is larger for $\alpha = 0$. The gray dashed line represents the baseline energy consumption when the readout does not interact with the signal, for $a = 0$. In this figure, $D_i = 1/\tau_i$ for $i = \eta,\ z,\ x$, $W_\eta = -1$, $\sigma = 1.5$, $\tau_\eta = 3\tau_z$, $\tau_z = \tau_x = 1$.

readout and the signal, this remains a feasible estimation with counting statistics alone. In Fig. 3(a), we plot the optimal readout coupling as a function of the strategy λ for different values of α. When $\mathcal{T}_x + \mathcal{T}_z$ is used by the sensor, the optimal coupling matches the one obtained in the ideal case where the entire entropy production $\dot{S}$ is known. When only $\mathcal{T}_x$ is employed and $\alpha \neq 0$, on the other hand, $a_{\rm opt}$ becomes systematically larger due to the fact that the sensor underestimates the dissipation. Furthermore, as α decreases, the strategy needs to be more and more information-driven for $a_{\rm opt}$ to be different from zero. This suggests that the regulatory mechanism is effectively increasing the cost of acquiring information, pushing λ_c to higher values. In the End Matter, we show that the same qualitative behaviour is recovered when the inhibitory regulation is implemented through z modulating the hidden chemical activity η.

Finally, we set a given energy budget, i.e., we fix the total energy consumption of the system $\dot{S} = \dot{S}^*$, which in turn determines the strategy of the sensor, and assess the performance of the optimal coupling by evaluating the information between the readout and the hidden process, $I_{x\eta}$. We recall that, although $I_{x\eta}$ cannot be measured directly, it is the ideal target that the sensor wants to maximize. In Fig. 3(b), we plot $I_{x\eta}$ against $\dot{S}^*$ up to the value corresponding to $\lambda = 0.9$. When $\alpha = 0$, there is no regulatory mechanism in place and the sensor can efficiently use energy to harvest information. However, as α decreases, the maximum value of $I_{x\eta}$ achievable at increasing energy budget becomes smaller for the same set of strategies. Remarkably, this behavior is still optimal in terms of the limited observability of the system, that is, the strategy being equal, the sensor tunes the readout coupling to account for the increased cost of information and aims at reducing $\dot{S}^*$ accordingly.

Overall, we have shown that trajectory-based estimates relying on counting statistics can be successfully implemented using pointwise mutual information and dissipation estimation via the traffic. This is particularly relevant when not all of the degrees of freedom can be observed, as in the case of the sensor studied here. Furthermore, such estimates can be exploited to balance information and dissipation during sensing processes. Despite our focus on a chemical network, this conceptual framework is in principle applicable to any artificial or biological system operating under similar constraints, especially multiscale ones [30,58,59] or coupled to shared changing environments [4,9,60,61]. We remark here that information maximization and dissipation minimization may not be general driving principles, as these two quantities are not necessarily in trade-off [62]. Nevertheless, several studies have shown that they appear in different contexts, either separately or together, from sensory adaptation [22,63] to bacterial chemotaxis [64,65] and chemical networks [11,43]. Our approach outlines a concrete path toward testing the relevance of these principles in biological systems, where the balance between energy consumption and information gathering can be incorporated as a plausible estimate from observed stochastic trajectories. In future works, it will be interesting to replace the mutual information with other quantities that can be measured in the presence of high-dimensional signals, where reliably estimating empirical probabilities becomes increasingly harder. Moreover, the application of these ideas to detailed signaling networks, where the sensor is realized through specific chemical motifs, is a fascinating possibility that may lead to uncovering the specific information-theoretic and thermodynamic role of known biochemical couplings. We believe that this Letter provides explicit evidence that, under physically relevant constraints, balancing information and dissipation might be an implementable design principle to perform adaptive strategies in biological and biochemical systems.

Acknowledgments—The authors thank Marco Baiesi, Matteo Ciarchi, and Vincenzo Maria Schimmenti for useful discussions. The authors thank the Max Planck Institute for the Physics of Complex Systems for hosting G. N. and D. M. B. during the initial phase of this work, and the International Center for Theoretical Physics for hosting D. M. B. during the final phase of this work. D. M. B. is funded by the program STARS@UNIPD with the project "ActiveInfo."

Data availability—The data that support the findings of this article are not publicly available. The data are available from the authors upon reasonable request.

[1] C. G. Bowsher and P. S. Swain, Environmental sensing, information transfer, and cellular decision-making, Curr. Opin. Biotechnol. **28**, 149 (2014).

[2] G. Reddy, A. Celani, T. J. Sejnowski, and M. Vergassola, Learning to soar in turbulent environments, Proc. Natl. Acad. Sci. U.S.A. **113**, E4877 (2016).

[3] G. Balázsi, A. Van Oudenaarden, and J. J. Collins, Cellular decision making and biological noise: From microbes to mammals, Cell **144**, 910 (2011).

[4] O. Karin and U. Alon, Temporal fluctuations in chemotaxis gain implement a simulated-tempering strategy for efficient navigation in complex environments, IScience **24** (2021).

[5] T. Nakajima, Biologically inspired information theory: Adaptation through construction of external reality models by living systems, Prog. Biophys. Molec. Biol. **119**, 634 (2015).

[6] H.-W. Wang, C. J. Wysocki, and G. H. Gold, Induction of olfactory receptor sensitivity in mice, Science **260**, 998 (1993).

[7] V. Sourjik and H. C. Berg, Receptor sensitivity in bacterial chemotaxis, Proc. Natl. Acad. Sci. U.S.A. **99**, 123 (2002).

[8] P. R. ten Wolde, N. B. Becker, T. E. Ouldridge, and A. Mugler, Fundamental limits to cellular sensing, J. Stat. Phys. **162**, 1395 (2016).

[9] T. Mora and I. Nemenman, Physical limit to concentration sensing in a changing environment, Phys. Rev. Lett. **123**, 198101 (2019).

[10] T. Tohme, M. Vergassola, T. Mora, and A. M. Walczak, Fast decisions with biophysically constrained gene promoter architectures, PRX Life **4**, 013009 (2026).

[11] C. C. Govern and P. R. ten Wolde, Energy dissipation and noise correlations in biochemical sensing, Phys. Rev. Lett. **113**, 258102 (2014).

[12] S. Liang, P. De Los Rios, and D. M. Busiello, Thermodynamic bounds on symmetry breaking in linear and catalytic biochemical systems, Phys. Rev. Lett. **132**, 228402 (2024).

[13] T. E. Ouldridge, C. C. Govern, and P. R. ten Wolde, Thermodynamics of computational copying in biochemical systems, Phys. Rev. X **7**, 021004 (2017).

[14] J. M. Parrondo, J. M. Horowitz, and T. Sagawa, Thermodynamics of information, Nat. Phys. **11**, 131 (2015).

[15] I. Lestas, G. Vinnicombe, and J. Paulsson, Fundamental limits on the suppression of molecular fluctuations, Nature (London) **467**, 174 (2010).

[16] A. Solopova, J. Van Gestel, F. J. Weissing, H. Bachmann, B. Teusink, J. Kok, and O. P. Kuipers, Bet-hedging during bacterial diauxic shift, Proc. Natl. Acad. Sci. U.S.A. **111**, 7427 (2014).

[17] M. Basan, S. Hui, H. Okano, Z. Zhang, Y. Shen, J. R. Williamson, and T. Hwa, Overflow metabolism in *Escherichia coli* results from efficient proteome allocation, Nature (London) **528**, 99 (2015).

[18] M. J. Falk, J. Wu, A. Matthews, V. Sachdeva, N. Pashine, M. L. Gardel, S. R. Nagel, and A. Murugan, Learning to learn by using nonequilibrium training protocols for adaptable materials, Proc. Natl. Acad. Sci. U.S.A. **120**, e2219558120 (2023).

[19] S. Okumura, G. Gines, N. Lobato-Dauzier, A. Baccouche, R. Deteix, T. Fujii, Y. Rondelez, and A. J. Genot, Nonlinear decision-making with enzymatic neural networks, Nature (London) **610**, 496 (2022).

[20] P. Sartori, L. Granger, C. F. Lee, and J. M. Horowitz, Thermodynamic costs of information processing in sensory adaptation, PLoS Comput. Biol. **10**, e1003974 (2014).

[21] G. Nicoletti and D. M. Busiello, Tuning transduction from hidden observables to optimize information harvesting, Phys. Rev. Lett. **133**, 158401 (2024).

[22] G. Nicoletti, M. Bruzzone, S. Suweis, M. Dal Maschio, and D. M. Busiello, Optimal information gain at the onset of habituation to repeated stimuli, eLife **13** (2025).

[23] A. J. Tjalma, V. Galstyan, J. Goedhart, L. Slim, N. B. Becker, and P. R. Ten Wolde, Trade-offs between cost and information in cellular prediction, Proc. Natl. Acad. Sci. U.S.A. **120**, e2303078120 (2023).

[24] D. Hartich, A. C. Barato, and U. Seifert, Nonequilibrium sensing and its analogy to kinetic proofreading, New J. Phys. **17**, 055026 (2015).

[25] M. Skoge, S. Naqvi, Y. Meir, and N. S. Wingreen, Chemical sensing by nonequilibrium cooperative receptors, Phys. Rev. Lett. **110**, 248102 (2013).

[26] H. Chang and A. Levchenko, Adaptive molecular networks controlling chemotactic migration: Dynamic inputs and selection of the network architecture, Phil. Trans. R. Soc. B **368**, 20130117 (2013).

[27] A. Levchenko and I. Nemenman, Cellular noise and information transmission, Curr. Opin. Biotechnol. **28**, 156 (2014).

[28] R. Fan and A. Hilfinger, Characterizing the nonmonotonic behavior of mutual information along biochemical reaction cascades, Phys. Rev. E **110**, 034309 (2024).

[29] M. K. Kajita, K. Aihara, and T. J. Kobayashi, Balancing specificity, sensitivity and speed of ligand discrimination by zero-order ultraspecificity, Phys. Rev. E **96**, 012405 (2017).

[30] J. Paulsson, O. G. Berg, and M. Ehrenberg, Stochastic focusing: Fluctuation-enhanced sensitivity of intracellular regulation, Proc. Natl. Acad. Sci. U.S.A. **97**, 7148 (2000).

[31] I. Di Terlizzi, Force-free kinetic inference of entropy production, Phys. Rev. Lett. **135**, 237101 (2025).

[32] C. Gardiner, *Stochastic Methods* (Springer, Berlin, Heidelberg, 2009), Vol. 4.

[33] L. Cantini, C. Cianci, D. Fanelli, E. Massi, and L. Barletti, Linear noise approximation for stochastic oscillations of intracellular calcium, J. Theor. Biol. **349**, 92 (2014).

[34] R. Grima, Linear-noise approximation and the chemical master equation agree up to second-order moments for a class of chemical systems, Phys. Rev. E **92**, 042124 (2015).

[35] R. Cheong, A. Rhee, C. J. Wang, I. Nemenman, and A. Levchenko, Information transduction capacity of noisy biochemical signaling networks, Science **334**, 354 (2011).

[36] W. Ma, A. Trusina, H. El-Samad, W. A. Lim, and C. Tang, Defining network topologies that can achieve biochemical adaptation, Cell **138**, 760 (2009).

[37] J. Selimkhanov, B. Taylor, J. Yao, A. Pilko, J. Albeck, A. Hoffmann, L. Tsimring, and R. Wollman, Accurate

information transmission through dynamic biochemical signaling networks, Science **346**, 1370 (2014).
[38] N. Barkai and S. Leibler, Robustness in simple biochemical networks, Nature (London) **387**, 913 (1997).
[39] M. Kollmann, L. Løvdok, K. Bartholomé, J. Timmer, and V. Sourjik, Design principles of a bacterial signalling network, Nature (London) **438**, 504 (2005).
[40] Y. Tu, Quantitative modeling of bacterial chemotaxis: signal amplification and accurate adaptation, Annu. Rev. Biophys. **42**, 337 (2013).
[41] M. Inoue and K. Kaneko, Cooperative adaptive responses in gene regulatory networks with many degrees of freedom, PLoS Comput. Biol. **9**, e1003001 (2013).
[42] T. M. Pham and K. Kaneko, Dynamical theory for adaptive systems, J. Stat. Mech. (2024) 113501.
[43] S. Flatt, D. M. Busiello, S. Zamuner, and P. De Los Rios, ABC transporters are billion-year-old Maxwell demons, Commun. Phys. **6**, 205 (2023).
[44] J. Agudo-Canalejo and R. Golestanian, Active phase separation in mixtures of chemically interacting particles, Phys. Rev. Lett. **123**, 018101 (2019).
[45] S. A. Loos and S. H. Klapp, Irreversibility, heat and information flows induced by non-reciprocal interactions, New J. Phys. **22**, 123051 (2020).
[46] T. Suchanek, K. Kroy, and S. A. Loos, Entropy production in the nonreciprocal Cahn-Hilliard model, Phys. Rev. E **108**, 064610 (2023).
[47] Z. Zhang and R. Garcia-Millan, Entropy production of nonreciprocal interactions, Phys. Rev. Res. **5**, L022033 (2023).
[48] A. Dinelli, J. O'Byrne, A. Curatolo, Y. Zhao, P. Sollich, and J. Tailleur, Non-reciprocity across scales in active mixtures, Nat. Commun. **14**, 7035 (2023).
[49] D. M. Busiello, M. Ciarchi, and I. Di Terlizzi, Unraveling active baths through their hidden degrees of freedom, Phys. Rev. Res. **6**, 013190 (2024).
[50] T. M. Pham, A. Alonso, and K. Proesmans, Irreversibility in non-reciprocal chaotic systems, New J. Phys. **27**, 023003 (2025).
[51] K. Sekimoto, Langevin equation and thermodynamics, Prog. Theor. Phys. Suppl. **130**, 17 (1998).
[52] A. Frishman and P. Ronceray, Learning force fields from stochastic trajectories, Phys. Rev. X **10**, 021009 (2020).
[53] C. Maes, K. Netočný, and B. Wynants, Steady state statistics of driven diffusions, Physica (Amsterdam) **387A**, 2675 (2008).
[54] M. Baiesi and G. Falasco, Inflow rate, a time-symmetric observable obeying fluctuation relations, Phys. Rev. E **92**, 042162 (2015).
[55] I. D. Terlizzi, M. Gironella, D. Herraez-Aguilar, T. Betz, F. Monroy, M. Baiesi, and F. Ritort, Variance sum rule for entropy production, Science **383**, 971 (2024).
[56] I. Di Terlizzi, M. Baiesi, and F. Ritort, Variance sum rule: Proofs and solvable models, New J. Phys. **26**, 063013 (2024).
[57] O. Shoval, H. Sheftel, G. Shinar, Y. Hart, O. Ramote, A. Mayo, E. Dekel, K. Kavanagh, and U. Alon, Evolutionary trade-offs, pareto optimality, and the geometry of phenotype space, Science **336**, 1157 (2012).
[58] G. Nicoletti and D. M. Busiello, Information propagation in multilayer systems with higher-order interactions across timescales, Phys. Rev. X **14**, 021007 (2024).
[59] G. Nicoletti and D. M. Busiello, Information propagation in Gaussian processes on multilayer networks, J. Phys. Complexity **5**, 045004 (2024).
[60] G. Nicoletti and D. M. Busiello, Mutual information disentangles interactions from changing environments, Phys. Rev. Lett. **127**, 228301 (2021).
[61] G. Malaguti and P. R. Ten Wolde, Theory for the optimal detection of time-varying signals in cellular sensing systems, eLife **10**, e62574 (2021).
[62] M. Baiesi and C. Maes, Life efficiency does not always increase with the dissipation rate, J. Phys. Comm. **2**, 045017 (2018).
[63] G. Lan, P. Sartori, S. Neumann, V. Sourjik, and Y. Tu, The energy–speed–accuracy trade-off in sensory adaptation, Nat. Phys. **8**, 422 (2012).
[64] H. H. Mattingly, K. Kamino, B. B. Machta, and T. Emonet, *Escherichia coli* chemotaxis is information limited, Nat. Phys. **17**, 1426 (2021).
[65] D. Hathcock, Q. Yu, B. A. Mello, D. N. Amin, G. L. Hazelbauer, and Y. Tu, A nonequilibrium allosteric model for receptor-kinase complexes: The role of energy dissipation in chemotaxis signaling, Proc. Natl. Acad. Sci. U.S.A. **120**, e2303115120 (2023).
[66] C. Maes, On the origin and the use of fluctuation relations for the entropy, Sémin. Poincaré **2**, 29 (2003).
[67] U. Seifert, Stochastic thermodynamics, fluctuation theorems and molecular machines, Rep. Prog. Phys. **75**, 126001 (2012).
[68] L. Peliti and S. Pigolotti, *Stochastic Thermodynamics: An Introduction* (Princeton University Press, Princeton, NJ, 2021).
[69] G. Gallavotti and E. G. D. Cohen, Dynamical ensembles in nonequilibrium statistical mechanics, Phys. Rev. Lett. **74**, 2694 (1995).
[70] G. E. Crooks, Entropy production fluctuation theorem and the nonequilibrium work relation for free energy differences, Phys. Rev. E **60**, 2721 (1999).

End Matter

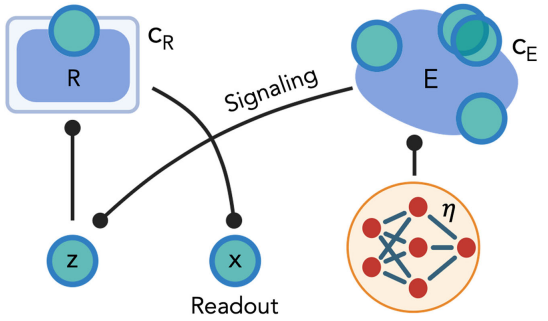

FIG. 4. Scheme of the chemical model. Internal species $\boldsymbol{H}$, readout X, and signaling molecule Z [whose fluctuations are in lowercase letters, $\boldsymbol{\eta}(t)$, $x(t)$, and $z(t)$] are coupled together only through intermediate fast complexes.

An exemplary signaling model—Here, we introduce a chemical network that plays the role of an elementary example of the class of systems studied in this Letter. The internal dynamics producing a signaling molecule Z is

$$\sum_j \alpha_j H_j \rightleftharpoons \sum_j \beta_j H_j$$
$$\sum_j \gamma_j H_j + E \rightleftharpoons C_E \to E + Z,$$

where we maintain full generality for the internal dynamics of H_i species, and we propose a simple, yet general, form of the process producing Z, i.e., an enzyme E catalyzing the conversion of internal molecules through an intermediate complex C_E. Then, Z can interact with a membrane receptor R to generate X via the complex C_R,

$$Z + R \rightleftharpoons C_R \to R + X \quad X \to \varnothing,$$

where the rightmost reaction represents a degradation dynamics. The associated stochastic evolution for concentrations (uppercase letters) can be obtained via Kramers-Moyal expansion [32] and feature nonlinear reaction terms and nondiagonal multiplicative noises.

We first incorporate the conservation laws $R(t) = R_{\mathrm{tot}} - C_R(t)$ and $E(t) = E_{\mathrm{tot}} - C_E$. Since typically complexes are fast variables, as for nucleotide-exchange and several enzyme kinetics [12,43], the chemical system has a layered structure as in Fig. 4. Since all couplings between $\boldsymbol{H}$, X, and Z are mediated by fast species, by writing down the Fokker-Planck equation, and integrating out C_R and C_E (with no-flux boundary conditions for all species), we obtain a new dynamics that only features diagonal multiplicative noise terms in Z and X. Indeed, there are no reactions (hence no noise) directly mixing $\boldsymbol{H}$, Z, and X (see Fig. 4). Moreover, the drift terms will depend on the average of C_E and C_R that, in the timescale separation regime, only depend on $\boldsymbol{\eta}$ and Z, respectively. The structure of the resulting dynamics resembles the one presented in Eq. (1). We remark here that we are only interested in motivating the use of our minimal model, without drawing any detailed connection between microscopic and effective parameters, since this will depend on the entire chemical dynamics.

The presence of a negative feedback from X on Z can also be implemented through a reaction,

$$X + R \rightleftharpoons C_R, \tag{A1}$$

where the additional (fast) complex formation effectively modifies the concentration of Z when integrated out.

For simplicity, limited resolution is added on top of the linearized dynamics to capture the ability to resolve only a certain range of fluctuations. While phenomenological at this stage, a similar threshold dynamics emerges in the microscopic model as a consequence of the saturating behavior of C_R as a function of z. We also note that our results can be immediately extended to multiple hidden signals. Indeed, since the properties of $\boldsymbol{\eta}$ enter in $\dot{S}|_{a=0}$, they do not influence the optimization over a.

Entropy production and kinetic inference—Consider a general overdamped Langevin dynamics,

$$\dot{\boldsymbol{x}} = \boldsymbol{A}(\boldsymbol{x}) + \sqrt{2\boldsymbol{D}}\boldsymbol{\xi}, \qquad \langle \xi_i(t)\xi_j(s)\rangle = \delta_{ij}\delta(t-s), \tag{B1}$$

with drift $\boldsymbol{A}(\boldsymbol{x})$ and diffusion matrix $\boldsymbol{D}$. The associated Fokker-Planck equation reads

$$\partial_t p(\boldsymbol{x}) = -\nabla \cdot \boldsymbol{j}(\boldsymbol{x}), \tag{B2}$$

and in a nonequilibrium steady state one has $\partial_t p(\boldsymbol{x}) = 0$ and a nonvanishing solenoidal probability current $\boldsymbol{j}(\boldsymbol{x}) = [\boldsymbol{A}(\boldsymbol{x}) - \nabla\phi(\boldsymbol{r})]p(\boldsymbol{x}) \neq 0$, $\nabla \cdot \boldsymbol{j}(\boldsymbol{x}) = 0$. The nonequilibrium steady state is characterized by a constant rate of entropy production $\dot{S}$ [66–70], which corresponds to the heat dissipated into the environment [51],

$$\dot{S} = \langle \boldsymbol{D}^{-1}\boldsymbol{A}(\boldsymbol{x}) \circ \dot{\boldsymbol{x}} \rangle. \tag{B3}$$

Estimating $\boldsymbol{A}(\boldsymbol{x})$ from trajectories is often impractical, motivating alternative approaches to infer dissipation. A particularly useful one is a kinetic decomposition of the entropy production [31,52,53],

$$\dot{S} = 4\mathcal{T} + \mathcal{G}, \tag{B4}$$

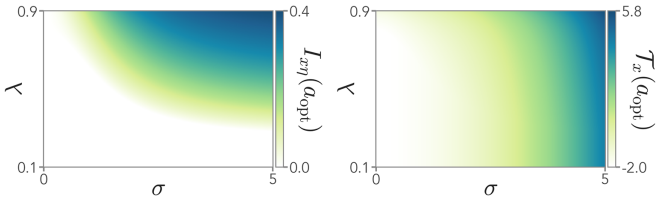

FIG. 5. $I_{x\eta}$ and $\mathcal{T}_x$ evaluated on the optimal coupling $a_{\rm opt}(\lambda,\sigma)$ in the infinite resolution limit, with $D_i = 1/\tau_i$, $W_\eta = -1$, $\tau_\eta = 3\tau_z$, $\tau_z = \tau_x = 1$.

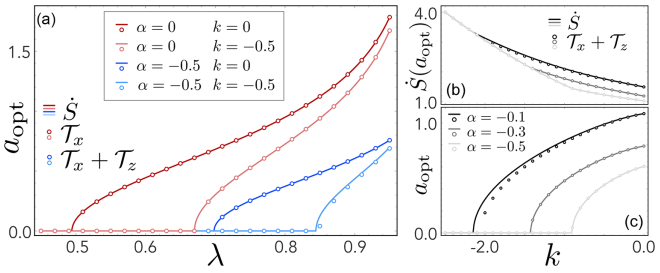

FIG. 6. (a) $a_{\rm opt}$ as a function of λ. As α and k increase, the critical value λ_c below which $a_{\rm opt} = 0$ increases. Lines represent results obtained by using the exact dissipation in the functional, while dots indicate those resulting from using traffic. For $\alpha = 0$, only $\mathcal{T}_x$ is needed, while the estimation of dissipation is approximate when $\alpha \neq 0$ and $k \neq 0$. (b) $\dot{S}$ evaluated on $a_{\rm opt}$ as a function of k shows that the traffic provides a good estimation of dissipation in a wide range of parameters. Deviations in $a_{\rm opt}$ can be easily appreciated (c). The other parameters are as in Fig. 3.

which expresses $\dot{S}$ in terms of two quantities that can, in principle, be inferred from time-series data. The *traffic* $\mathcal{T}$ quantifies the time-symmetric dynamical activity, whereas the *inflow rate* $\mathcal{G}$ [54] captures the local compression or expansion of probability. Using a recently introduced variance sum rule [31,55], the traffic becomes

$$\mathcal{T} = -\frac{1}{4}(D^{-1})_{ij}\ddot{C}^{(r)}_{ij}(0), \tag{B5}$$

where $C^{(r)}_{ij}(t) = \langle r_i(t) r_j(0)\rangle - \langle r_i\rangle\langle r_j\rangle$ is the covariance matrix of the observed trajectory $\boldsymbol{r}(t)$. Diffusion coefficients entering Eq. (B5) are also accessible from short-time statistics: $D_{ij} = -(\dot{C}^{(r)}_{ij} + \dot{C}^{(r)}_{ji})/2$. On the other hand, the inflow rate can be both expressed in terms of $\nabla\phi = -\nabla \log p(\boldsymbol{r})$, which can be estimated from trajectories, as well as in terms of the divergence of the drift,

$$\mathcal{G} = D_{ij}C^{\nabla\phi}_{ij}(0) = -\int d\boldsymbol{r}\, p(\boldsymbol{r})\partial_i A_i(\boldsymbol{r}), \tag{B6}$$

showing that, in our model (2), the inflow rate is not affected by the cross couplings and by a in particular. Furthermore, $D_{ij} = D_i\delta_{ij}$ in the observable quantities, and the sensor modifies only the coupling between the signaling molecule Z and the readout X. Therefore, since we are interested in estimating the entropy production induced by the nonreciprocity of a,

$$\dot{S}_a = \dot{S} - \dot{S}|_{a=0}, \tag{B7}$$

the only surviving terms are those affected by a modification in the value of the coupling a. As such, the only relevant terms are $\mathcal{T}_x$ and $\mathcal{T}_z$. Consequently,

$$\dot{S}_a = 4[(\mathcal{T}_x + \mathcal{T}_z) - (\mathcal{T}_x + \mathcal{T}_z)|_{a=0}]. \tag{B8}$$

If either a feedback from X to Z or from Z to H is present, this result is exact, otherwise it is approximate. Also, if no feedback from X to Z is implemented, the only relevant term is $\mathcal{T}_x$, since $\mathcal{T}_z$ would not depend on a. Numerically, we estimate the traffic using autocorrelation functions and their derivatives via finite differences.

Exact results in the infinite resolution limit—In the infinite resolution limit, Eq. (2) reduces to an Ornstein-Uhlenbeck process with interaction matrix,

$$\boldsymbol{A} = \begin{pmatrix} W_\eta/\tau_\eta & 0 & 0 \\ \sigma & -1/\tau_z & \alpha a \\ 0 & a & -1/\tau_x \end{pmatrix}, \tag{C1}$$

and a block-diagonal diffusion matrix $\boldsymbol{D} = \mathrm{diag}(D_\eta, D_z, D_x)$. The covariance matrix $\boldsymbol{\Sigma}$ of the entire system obeys the Lyapnuov equation $\boldsymbol{A\Sigma} + \boldsymbol{\Sigma A}^T = -2\boldsymbol{D}$ and can be found analytically. Then, if $T_{\rm obs}$ is also large and we can neglect sampling errors, the components of traffic estimated from the stochastic trajectories become exact and are given by the diagonal elements of the matrix $\boldsymbol{\Xi} = \boldsymbol{D}^{-1}\boldsymbol{A\Sigma A}^T$. In particular, in the main text we considered $4\mathcal{T}_x = \Xi_{xx}$ and $4\mathcal{T}_z = \Xi_{zz}$, whereas the entropy production if $\dot{S} = \mathrm{Tr}\boldsymbol{\Xi} - \mathrm{Tr}\boldsymbol{A}$. In this limit, on the other hand, the average of the pointwise mutual information in the $T_{\rm obs} \to \infty$ limit becomes

$$I_{xz} = \frac{1}{2}\log\frac{\Sigma_{xx}\Sigma_{zz}}{\Sigma_{xx}\Sigma_{zz} - \Sigma^2_{xz}} \tag{C2}$$

and similarly for $I_{x\eta}$ [21]. In Fig. 5 we show $I_{x\eta}$ and $\mathcal{T}_x$ in the (σ,λ) plane when evaluated on $a_{\rm opt}$ obtained from Eq. (8). Despite the fact that $a_{\rm opt}$ may be nonmonotonic as a function of σ [see Fig. 2(a)], $I_{x\eta}$ and $\mathcal{T}_x$ are not, suggesting that such nonmonotonicity serves to balance information and dissipation in the Pareto optimization.

Feedback between signal and hidden activity—In analogy to the coupling between X and Z, an additional negative feedback mechanism connecting Z and $\boldsymbol{H}$ can also be incorporated into the model through the reaction

$$C_E \rightleftharpoons E + Z. \tag{D1}$$

Proceeding as above, this results in a coupling term $-\boldsymbol{k}z$ appearing in the dynamics of $\boldsymbol{\eta}$. Notice that a similar term can equally be implemented through different biochemical mechanisms [22,35–40]. In this case, the estimation of the traffic associated with the readout, $\mathcal{T}_x$, is sufficient to have a precise estimation of dissipation. In Fig. 6(a), we show that this regulatory mechanism has an analogous role as the interaction between X and Z. By increasing its strength k, the cost for the sensor of acquiring information increases, thereby pushing the strategy to be more information-driven to achieve a given a_{opt}.

In the most complex scenario, where both regulations are simultaneously present, i.e., $\alpha \neq 0$ and $k \neq 0$, the sensor can estimate the dissipation through $\mathcal{T}_x + \mathcal{T}_z$ only approximately. However, in Figs. 6(b) and 6(c) we show that the inference remains robust over a wide range of parameters and, most importantly, that the role of the inhibitory mechanisms remains unchanged: increasing either α or k, or both, results in a higher cost of acquiring information for the sensor [see Fig. 6(a)].